Nuclear Data for Science and Technology (1988 MITO), 1107-1114, Copyright © 1988 JAERI.

NEUTRON CAPTURE RATES FOR STELLAR NUCLEOSYNTHESIS

F. Käppeler

Kernforschungszentrum Karlsruhe, Institut für Kernphysik,
D-7500 Karlsruhe, Federal Republic of Germany

Abstract: The quantitative description of neutron capture nucleosynthesis requires the neutron capture cross sections of all involved isotopes. Only with this data base the observed abundances can be interpreted in terms of the physical conditions prevailing at the respective stellar sites. In this contribution, importance and status of stellar capture rates for the s- and r-process are outlined. The role of model calculations is emphasized as an essential complement to laboratory measurements, e.g. for determining the cross sections of short-lived isotopes that are not accessible to present experimental techniques as well as for describing the influence of temperature. The latter may cause the stellar rates to deviate significantly from laboratory values. Possible experimental improvements are discussed in connection with new developments in detector techniques and neutron sources.

(nucleosynthesis, s- and r-process, neutron capture cross sections, 1 < En < 200 keV)

1. Neutron Physics and the Stellar Interior

The synthesis of the chemical elements heavier than iron can be understood only via neutron capture processes in stars; fusion reactions between charged particles do not contribute in this mass region because of the increasing Coulomb barriers and the decreasing binding energies per nucleon. The great variety of nuclei involved in these processes carries detailed information on the peculiarities of their formation. To decipher this puzzle in terms of the stellar mechanisms is an exciting aspect of neutron physics. Most interesting in this respect are a number of nuclei between iron and the actinides the abundances of which depend sensitively on the physical conditions under which they were produced. In turn, it should therefore be possible to deduce these physical conditions if the observed abundances can be described by the underlying neutron physics.

This type of argument was already used in the classical paper by Burbidge et al.[1] in order to identify the various processes of relevance in the mass range A > 70. These ideas are illustrated by the section of the chart of nuclides given in figure 1. The inset shows a rough sketch of the distribution of the chemical abundances in the solar system. It is known from astronomical observations that this distribution is typical not only for the sun and the milky way but also for all galaxies which could be examined. It is therefore called the cosmic or standard abundance distribution. As far as the heavy elements are concerned this distribution is characterized by a pronounced maximum at A = 56 and by a drastic decline towards higher mass numbers. This means that neutron capture was much less efficient in element synthesis than the fusion of charged particles.

Neutron capture nucleosynthesis starts at the abundance maximum which peaks at ^{56}Fe by successive neutron captures and subsequent beta decays. Aside from an odd-even fine structure (not shown in figure 1) the abundance distribution exhibits twin peaks at A ~130/140 and at ~195/208, while a third feature at A ~80/90 is not resolved. These maxima together with the isotopic patterns of the elements suggest the existence of two different neutron capture processes, the s- and the r-process. The s-process (s = slow neutron capture) is supposed to be characterized by low neutron densities, resulting in neutron capture times of the order several years. Hence, beta decays are usually faster when the neutron capture chain encounters an unstable isotope, causing the s-process to follow the valley of beta stability as indicated by the thick solid line in figure 1. The r-process (r = rapid neutron capture) is associated with an extremely high neutron density with capture times of the order milliseconds or faster. Because beta decays are much slower, the r-process path is shifted to extremely neutron-rich nuclei. The neutron capture chain is halted close to the neutron drip line by (γ,n)-reactions via thermal photons, until beta decay to the next element allows the reaction chain to move on.

This classification implies that the s-process is determined by the neutron capture cross sections of the isotopes involved; nuclei with small cross sections will act as bottle necks for the mass flow and will build up large abundances. Obviously, this occurs at magic neutron numbers, thus explaining the sharp abundance peaks at A ~90, 140, 208. The r-process abundances are independent of the capture cross sections to first approximation, but reflect the beta decay times at the 'waiting points'. The longest decay times occur again at neutron magic nuclei, but these are reached at smaller mass numbers, as indicated in figure 1 for N = 50. The corresponding abundance peaks originate from the decay of the r-process products and are shifted from the s-process peaks by about 10 mass units.

In general, the observed abundances are mixtures of contributions from the s- and r-process. Apart from the assignment of the abundance peaks, there are two ensembles of isotopes which can be attributed to the s- and r-process, respectively. Pure r-process nuclei are marked in figure 1 by dashed arrows: these nuclei terminate the beta decay chains from the r-process, but are not reached by the s-process because of their short-lived neighbors. In turn, they shield their stable isobars against the r-process, which therefore are of pure s-process origin (heavy boxes in figure 1). These two groups of nuclei represent important normalization points for any nucleosynthesis model in the mass region A > 70.

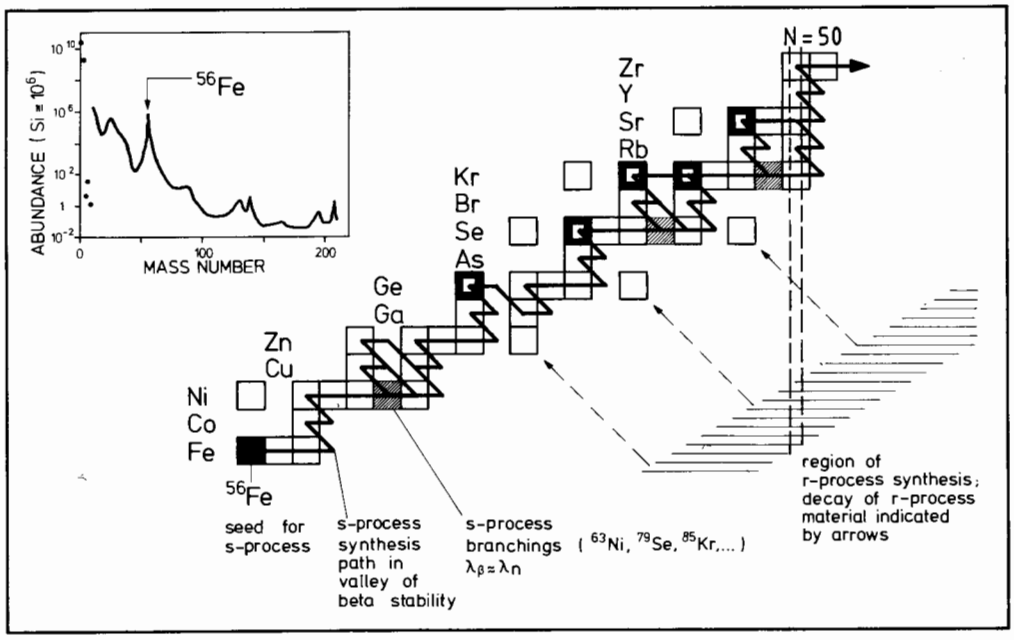

Fig.1 Section of the chart of nuclides illustrating the main features of nucleosynthesis in the mass region A > 70 (for details see text).

In addition to the **s**- and **r**-process, at least one other process has to be postulated in order to account for the neutron-poor isotopes, e.g. ^{74}Se, ^{78}Kr, and ^{84}Sr in figure 1. The abundances of these isotopes are about one order of magnitude smaller than those of the **s**- and **r**-process isotopes and are attributed to a **p**-process, where **p** stands for proton capture or photodesintegration. This process is not yet understood quantitatively, which presents a problem for future **s**-process studies because the **s**-only nuclei discussed above might require correction for **p**-process contributions in some cases (see section 4).

Finally, figure 1 illustrates an important feature of the **s**-process, the so-called **s**-process branchings. In spite of the neutron capture times being of the order years the beta decay times are not always faster. At some nuclei, competition between beta decay and neutron capture causes the **s**-process path to split. Such branch points are e.g. ^{63}Ni, ^{79}Se, and ^{85}Kr, which are shaded in figure 1. The abundance patterns in these branchings are sensitive to the physical conditions during the **s**-process; this is most obvious for the neutron density, but holds also for the temperature and the mass density. These problems will shortly be addressed in sections 3 and 4.

Based on the ideas outlined above, phenomenological models were developed for the **s**- and the **r**-process (sections 2 and 3). In these approaches, plausible stellar scenarios were approximated by idealized conditions. In order to identify the true conditions, the free model parameters were adjusted as to reproduce the observed abundances. This procedure was successful for the **s**-process, where the time scale is long enough to justify a steady solution, and where mostly stable isotopes are involved whose relevant properties can be studied in laboratory experiments. For the **r**-process the situation is more complicated because it occurs presumably in a stellar explosion, which can hardly be parameterized in a schematic way. An additional problem arises from the fact that the isotopes in the **r**-process region are practically unknown, and that extrapolation of their properties implies large uncertainties.

Realistic stellar models, that became available during the last 20 years, are very difficult to quantify. The **r**-process was proposed to occur in Novae and/or in Supernovae, but so far none of these attempts was able to satisfactorily reproduce the observed abundances. The main difficulty of these models originates from the complicated hydrodynamics of the associated explosion, which exceeds the capabilities of present day computers.

The **s**-process was long assumed to occur in helium burning zones during the late stages of stellar evolution when the stars expand to become Red Giants[1]. This was supported by astronomical observations, which showed that **s**-elements were enhanced in the atmospheres of these stars. A particularly convincing argument for this hypothesis was the discovery of technetium lines in the spectra of certain S-stars by Merrill[2]. As there are no stable Tc isotopes, and as the longest Tc half-life is much shorter than the age of Red Giants, this was direct evidence for ongoing **s**-processing in the interior of these stars. Various stellar models have been worked out in sufficient detail to allow for quantitative studies. The comparison with results from the classical model shows, however, that there are still many open problems, and that both approaches have to be further improved to solve the quest for the stellar **s**-process.

2. Cross Sections for the r-Process

If the neutron density in the r-process is sufficiently high, e.g. $>10^{20}$ n/cm^3, neutron capture is always faster than beta decay, and an equilibrium between (n,γ) and (γ,n) reactions is

achieved as the neutron capture chain approaches the neutron drip line. At the high temperatures in stellar explosions of ~10^9 K this point is reached, when the binding energies have decreased to ~2 MeV. Under this condition, a static r-process develops /3,4/, where the resulting abundances are completely determined by the beta decay times at the waiting points and where neutron capture cross sections are unimportant. Though it was possible to reproduce some of the abundance features of the r-process with this assumption, it was clear that a realistic model had to follow the associated explosion in time, i.e. to consider the time-dependence of temperature and neutron density. Such a dynamic r-process requires a detailed reaction network comprising several thousand nuclei in order to describe the freeze-out of the abundances at the end of the explosion. The most important neutron reactions in this network are capture and fission.

Any calculation of neutron reaction cross sections far from the stability line has to face the problem that there is no direct experimental information, neither on cross sections nor on nuclear properties, to compare with. This means, that the model parameters have to be extrapolated from the stability valley. In contrast to cross section calculations in the stability valley, where phenomenological parameter systematics can be applied[5], extrapolations to the far neutron rich side are more reliable, if they make use of realistic physical concepts.

In general, such calculations are based on the statistical model starting from the Hauser-Feshbach formula. The most recent model calculations for r-process applications[6] are performed with realistic optical model potentials (for particle transmission coefficients), and with improved prescriptions for the determination of nuclear level densities and of electric dipole transmission coefficients. These calculations were shown to reproduce the experimental data of stable nuclei within a factor of two. Nevertheless, considerable uncertainties remain for the extrapolation to nuclei on the r-process path. This includes screening corrections for reactions with charged particles in the incoming or outgoing channel, as well as the increasing importance of direct reactions. This latter point was emphasized in case of neutron capture rates[7]. The decreasing level densities near the r-process path result in rather small cross sections via the formation of a compound nucleus, so that the contribution from direct capture becomes a significant correction.

Experimental information on nuclei on or near the r-process path is very scarce. It was not until recently, that experiments at on-line mass separators succeeded to reach true r-process nuclei for the first time. From the measured beta decay properties of the waiting point nuclei ^{80}Zn /8,9/ and ^{130}Cd /10/ it seems possible to constrain the stellar conditions under which the r-process has operated[11]. This study indicates that the solar r-abundances resulted indeed from an (n,γ) - (γ,n) equilibrium, a situation which excludes r-process scenarios that are characterized by comparably low neutron densities, like explosive helium burning. However, further experimental efforts are necessary in order to quantify these results with improved nuclear physics data.

3. Cross Sections for the s-Process

Definition of stellar cross section

The s-process is supposed to operate in the helium burning zones during the late stages of stellar evolution. In such an environment, mass densities are ~1000 g/cm^3 and temperatures are between ~200 and 400 million degrees depending on the stellar mass. Under these conditions, neutrons can be produced via (α,n) reactions on ^{13}C or ^{22}Ne, which are then quickly thermalized, exhibiting a Maxwell-Boltzmann spectrum

$$\Phi \sim E_n \exp(-E_n/kT) \qquad (1)$$

with thermal energies around kT = 30 keV. The effective stellar cross section, $\langle\sigma\rangle$, is an average of the product of the cross section differential in energy, σ(En), and the relative velocity of neutron and target, v, over the thermal flux spectrum of equation (1). For astrophysical applications, $\langle\sigma\rangle$ is defined[12] as

$$\langle\sigma\rangle = \frac{\langle\sigma v\rangle}{v_T} = \frac{2}{\sqrt{\pi}} \frac{\int_0^\infty \sigma(E_n) E_n \exp(-E_n/kT) dE_n}{\int_0^\infty E_n \exp(-E_n/kT) dE_n} \qquad (2)$$

where En is the total kinetic energy in the center-of-mass system. The factor $2/\sqrt{\pi}$ comes from the fact that the mean thermal velocity $v_T = \sqrt{2kT/m}$, where m is the reduced mass, is used for normalization instead of the average velocity.

The definition of $\langle\sigma\rangle$ is convenient, because the stellar capture rate follows then as

$$\lambda_n = \langle\sigma\rangle n_n v_T \qquad (3)$$

where n_n is the neutron density. The definition of $\langle\sigma\rangle$ also implies that the stellar rate λ_n is rather insensitive to temperature because most differential capture cross sections scale with 1/v. Therefore, cross sections for s-process calculations are usually given for a standard thermal energy of kT = 30 keV.

Direct Detection Techniques

As illustrated in figure 2, neutron capture leads to excited states in the product nucleus. The capture cascade to the ground state is governed by statistics according to the decay channels of the particular level scheme. Therefore, the capture gamma-ray cascades may exhibit large fluctuations in multiplicity. The only well defined property is the total gamma-ray energy of the cascades, which

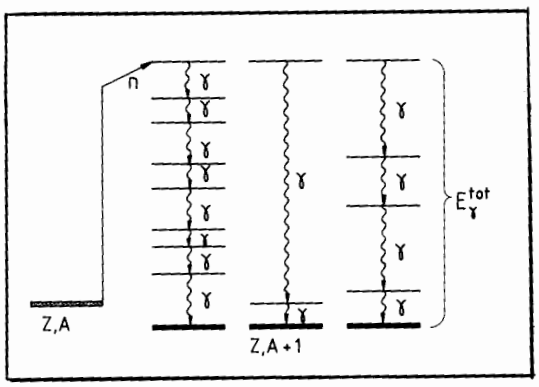

Fig.2 Gamma-ray cascades following neutron capture. The total cascade energy corresponds to the binding energy plus the kinetic energy of the neutron.

is the sum of the neutron binding energy and the kinetic energy of the captured neutron.

Consequently, the complete detection of all gamma-rays in a capture cascade with good energy resolution would represent the best signature for neutron capture events. Such a detector was first approximated by large liquid scintillator tanks. Due to their limited energy resolution and efficiency these detectors did not allow for complete separation of the capture events from background by sample scattered neutrons, leading to typical uncertainties of ~10% . Therefore, other techniques were favored in the seventies, which were based on the detection of only one single gamma-ray of the cascade. Correspondingly, a correction had to be made for the cascade multiplicity. This was achieved either by designing a detector with an efficiency that increased linearly with gamma-ray energy (Moxon-Rae detectors[13]) or by imposing this property to a detector by off-line weighting of an additional energy signal (total energy detectors[14]). These detectors were less affected by backgrounds and were shown to yield cross sections with uncertainties of 4 to 5% in favorable cases. However, this appears to be the limit of these detectors, as the correction for the cascade multiplicity implies an inherent uncertainty of that order. Recent efforts to investigate that point by experimental studies of the efficiency[15] seem to confirm these reservations.

The needs for more precise capture cross sections in various fields led back to the original idea of constructing a detector that can be operated as a calorimeter by summing over the entire capture cascade. The first 4π detector of this type, which in principle had sufficiently good resolution in gamma-ray energy was the ROMASCHKA detector[16], consisting of 48 NaI(Tl) modules of 180 l total volume. However, there were again problems with background from scattered neutrons, so that a massive ^{10}B shield had to be used around the sample. As this shield severely degraded the energy resolution, only multiplicity spectra were recorded with the ROMASCHKA detector. This problem could be solved when large BaF2 crystals became available, which exhibit superior features for use as detector material in neutron capture studies /17,18/. A 4π array built from BaF2 crystals has been set up at KfK Karlsruhe and is described at this conference[19]. With this new detector, capture cross section measurements on the 1 to 2% level are expected.

Activation Technique

Instead of measuring the capture cross sections as a function of neutron energy and folding the result with the stellar neutron spectrum, the effective stellar cross section could be obtained directly, if it were possible to reproduce the stellar spectrum in the laboratory. It has been demonstrated, that nuclear reactions can indeed yield spectra, which closely resemble a Maxwell-Boltzmann distribution typical for the **s**-process environment: The $^{7}Li(p,n)^{7}Be$ reaction at Ep = 1912 to 1914 keV yields a spectrum similar to that for kT = 25.0 ± 0.5 keV /20,21/, while the $^{3}H(p,n)^{3}He$ reaction at Ep = 1099 keV simulates that for kT = 52 keV[22]. In both cases, the proton energies are close enough at the reaction threshold, that the compound system moves faster than the neutrons in the center of mass system. Therefore, all neutrons are emitted in a forward cone with 120 deg opening angle.

Figure 3 illustrates the close correspondence of the angle-integrated spectrum from the $^{7}Li(p,n)^{7}Be$ reaction and the Maxwell-Boltzmann fit for kT = 24.7 keV. Only at neutron energies above 100 keV there are significant differences, but

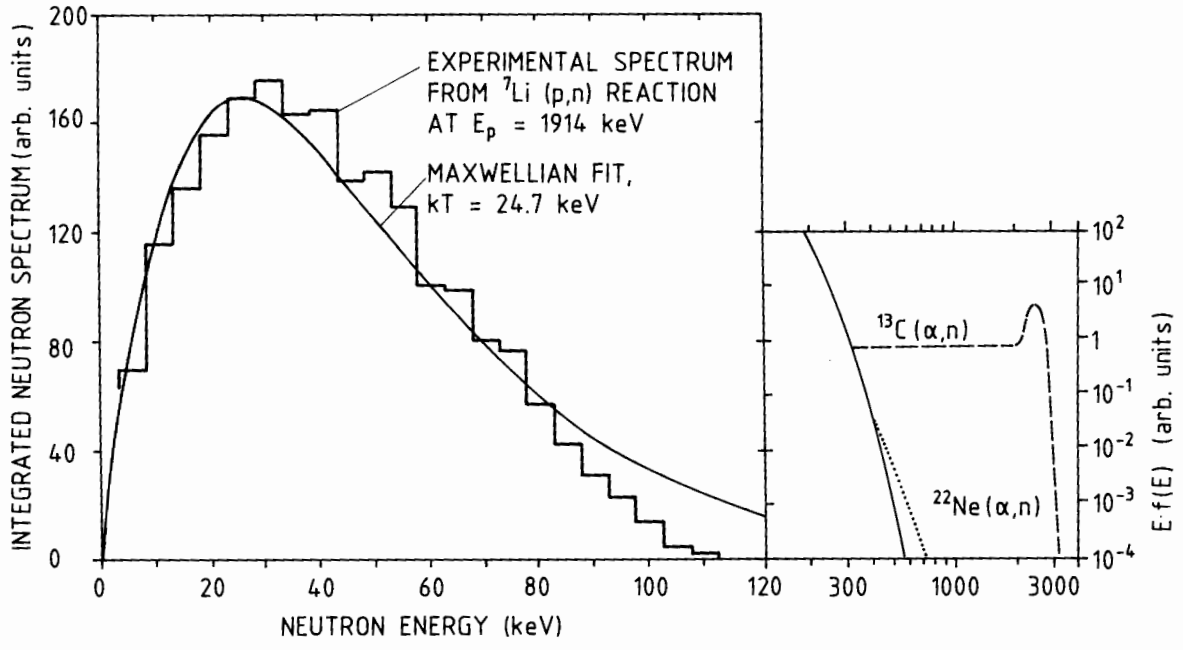

Fig.3 (left): Comparison of the stellar Maxwell-Boltzmann spectrum with the spectrum obtained from the $^{7}Li(p,n)^{7}Be$ reaction. The simulated spectrum allows for the direct measurement of stellar cross sections. (right): If the stellar neutron source is exoergic, the spectrum is not completely thermal but exhibits a 1/E tail that can affect the rate of those reactions, which are characterized by a threshold in the range 0.3 to 3 MeV.

these are of little influence on the stellar average. Because of the 1/v trend in most capture cross sections, the respective corrections cancel in first approximation, if cross sections are measured relative to a standard. However, in a few cases, where the cross sections exhibit widely spaced resonances, the stellar value might be affected by the energy range above 100 keV. Then, averaging measurements in the quasi-stellar spectrum must be checked at the higher energy of kT = 52 keV provided by the $^{3}H(p,n)^{3}He$ reaction or must be complemented by differential data above 100 keV.

The right part of figure 3 gives the extension of the stellar spectrum to higher energies. It was pointed out recently[23] that the neutrons produced in (α,n) reactions are not completely thermalized before they are captured. Depending on their production energy, there is a small fraction of epithermal neutrons. Though this is too small to affect the stellar neutron capture cross sections, it may cause an enhancement of (n,p) or (n,α) rates by many orders of magnitude, if the respective cross sections do have their thresholds in the critical energy range. Whether this effect is strong enough to ultimately affect the observed abundances is still open at present.

For capture cross section measurements, the quasi-stellar spectra are best suited in conjunction with the activation technique. The virtues of this method, i.e. its sensitivity and accuracy, make it an important complement to the direct detection techniques. Usually, relative measurements are performed using a sample sandwiched between gold foils. Gold is a convenient standard in this respect, as the decay of ^{198}Au offers a convenient half-life of 2.6 d and a strong gamma-line at 412 keV (I_γ = 95.5%). However, activation measurements can also be performed in an absolute way, if one makes use of the fact that each neutron produced via the $^{7}Li(p,n)^{7}Be$ reaction leaves a radioactive ^{7}Be nucleus. As all neutrons are emitted in forward direction, the entire flux penetrates the sample. This possibility has been used for absolute cross section measurements on gold /24, 25/, and was again used in a recent, precise determination of the stellar gold cross section[21]. In this study all relevant experiment parameters were carefully investigated in a series of activations, resulting ultimately in an overall uncertainty of 1.4% only. Hence, the gold cross section is the best known standard at keV neutron energies.

Besides the precision, which can be achieved with the activation technique, this method is of superior sensitivity as well. One of the smallest cross sections along the **s**-process chain is that of doubly magic ^{48}Ca. Its stellar cross section has been measured via activation to $\langle\sigma\rangle$ = 0.88±0.09 mb using only 15 to 40 mg of enriched CaCO3 samples[26]. If the experimental conditions of that measurement are extrapolated, one can estimate a sensitivity limit of ~1μb for capture cross section measurements with the activation technique. As all cross sections of relevance for the **s**-process are much larger, this limit just illustrates the potential of the technique with respect to those cases, where only small sample amounts and/or low isotopic enrichments are available.

Status of capture cross sections for the **s**-process

About 240 stable isotopes are involved in the **s**-process. A compilation of the available information on the respective capture cross sections[27] shows that about 90% of these nuclides have been investigated experimentally. However, this fraction reduces to 40% if one considers only those cases where an accuracy of better than 8% was reported. This limit corresponds to the capabilities of the modern techniques mentioned above and was usually achieved in more recent measurements.

The situation is very similar for the ensemble of isotopes, which are entirely or predominantly produced in the **s**-process, and which play a key role as normalization points for any **s**-process model. From the 40 important isotopes in this group there are 15 with uncertainties larger than 8% . It is obvious that the cross sections of these isotopes are of highest priority for further efforts to improve the data basis for **s**-process nucleosynthesis. Therefore, these nuclides are listed explicitely in table I. The only isotopes in this group, which are not yet measured are ^{128}Xe, ^{130}Xe, and ^{192}Pt, simply because the required amount of enriched material is not available.

Table I Requests for (n,γ) cross sections of key importance for **s**-process nucleosynthesis. Listed are cases, where present uncertainties exceed 8% ; data are from /21,27/.

stable isotopes		present stellar cross section (mb)	uncertainty (%)	unstable isotopes	calculated cross section (mb) local /6,38/	empirical /34/	global systematics /33/	/32/
^{58}Fe	exp.	12.8 ± 1.3	10%					
^{86}Kr	"	3.65 ± 0.30	8.5%	^{79}Se*	218±50 /35/	514	260	
^{88}Sr	"	6.2 ± 0.5	8%	^{85}Kr	67±17 /36/	25	150	
^{104}Pd	"	289 ± 29	11%	^{147}Pm*	1163 /37/	1135		1400
^{110}Cd	"	253 ± 30	12%	^{151}Sm*	1932 "	2809		1990
^{122}Te	"	295 ± 60	20%	^{163}Ho*		2264		2880
^{124}Te	"	162 ± 21	13%	^{170}Tm				2260
^{128}Xe	calc.	249	~25%	^{179}Ta				3250
^{130}Xe	"	153	~25%	^{185}W				794
^{134}Ba	exp.	221 ± 35	16%	^{205}Pb		83		58
^{136}Ba	"	69 ± 10	15%					
^{142}Nd	"	45.3 ± 3.8	8.5%					
^{154}Gd	"	1278 ± 102	8%					
^{192}Pt	calc.	388	>50%					
^{198}Hg	exp.	173 ± 15	9%					

* accessible to present techniques

With many cross sections for the **s**-process approaching the 5% level of accuracy, increasing attention has to be given to the cross sections of long-lived radioactive isotopes. As shown in section 1, these nuclei act as branching points for the **s**-process flow. The strength of a branching is determined by the respective rates for beta decay and neutron capture of the branch point isotope, and hence by its capture cross section. There are about 50 such isotopes on the **s**-process path, with ~30 of primary importance. So far, only very long-lived isotopes have been studied experimentally /28,29,30/, which exhibit low specific activities and soft radiations associated with the decay. The most important examples are included in table I with an asterix marking those cases, which might be accessible to present techniques. However, for most of these examples sufficient amounts of isotopically enriched sample material are not easily available.

Conventional techniques are limited to examples, where the specific activities of the sample do not cause too severe backgrounds, either because the half-lives are long enough or because the decay radiations can be sufficiently suppressed in the detection system. Otherwise, measurements can only be performed by improving on the neutron flux to override the sample-induced background. A powerful tool in this respect is the spallation neutron source at the proton storage ring of LAMPF in Los Alamos, where the detection limit for investigation of radioactive targets is boosted by more than a factor 1000 compared to existing facilities such as eletrostatic accelerators or electron linear accelerators. (For details of this facility see contribution IJ01[31]).

All cross sections, for which experimental information is still missing, have to be determined via model calculations. These calculations are performed with the statistical model, but differ in the treatment of the model parameters. By choosing a global parameter set for the whole periodic table, Holmes et al.[32] and Woosley et al.[33] were able to calculate a large number of cross sections, which agree with experimental values within a factor 2. This approach was improved by Harris[34] who applied experimental parameters and the evaluated systematics of Reffo[5]. Restricting the calculations to a rather small mass range, Reffo et al.[38] succeeded to refine the parameterization considerably. Their local parameter systematics were checked for internal consistency, and allowed for determining the cross sections with ~25% uncertainty in favorable cases.

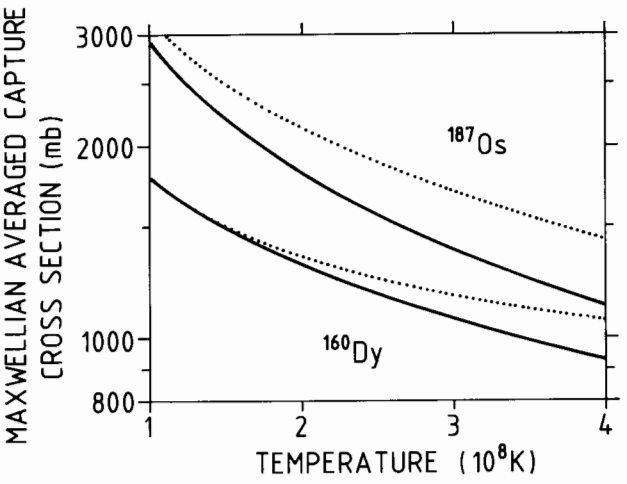

Fig.4 Stellar capture cross sections of ^{160}Dy and ^{187}Os versus temperature (dotted lines). Their dominance over the respective ground state values (solid lines) illustrates the effect of neutron capture in excited states.

Comparison of the calculated cross sections for the unstable isotopes in the right part of table I shows that there are severe discrepancies between the different model approaches. This is most obvious for the example of ^{85}Kr. As this nucleus is located at the shell closure with N = 50, the level density parameter becomes very uncertain unless it is carefully adjusted by means of a local systematics.

Stellar cross sections

Even if the progress in experimental techniques and neutron sources would provide reliable laboratory cross sections for all isotopes in the **s**-process chain, theoretical calculations will be indispensible in order to determine the differences between laboratory results and the true stellar values. Such differences result from the fact that low lying excited nuclear states will be populated in the hot stellar plasma, e.g. via photo- or Coulomb-excitation. The population probabilities are given by

$$p_i = Z^{-1}(2J_i+1)\exp(-E_i/kT) \qquad (4)$$

where

$$Z = \sum_m (2J_m+1)\exp(-E_m/kT) \qquad (5)$$

is the nuclear partition function with the sum running over all excited states. The stellar cross section is then the average over the cross sections from all states weighted with their population probabilities.

Usually, the difference to the laboratory cross section is small; but for low lying states with large spins the population probability as well as the cross section are enhanced, leading to a significant effect. This is shown in figure 4, where the temperature dependence of the cross sections of ^{160}Dy and ^{187}Os are plotted with and without the effect of the excited states, respectively. The effect of temperature is larger for ^{187}Os because its stellar cross section is dominated by the first excited (3/2-) state at 9.75 keV. Already at thermal energies of 20 keV (T = 2.3 10^8 K) this state is populated by 52% compared to 42% of the ground state (1/2-), because of its

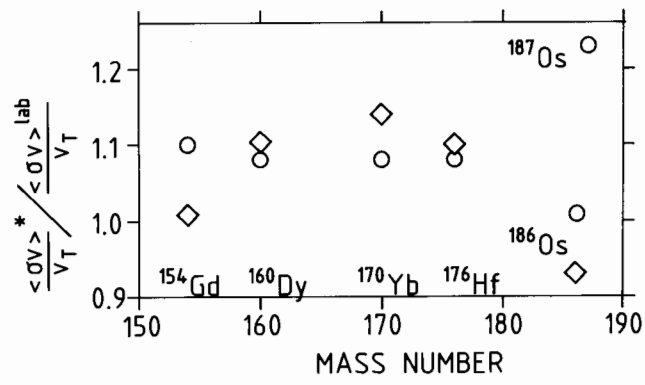

Fig.5 The ratio of stellar over laboratory cross section for those **s**-only isotopes, which show large effects. The symbols refer to Refs./33,34/ (o,□).

larger spin. In case of ^{160}Dy, the first excited state at 86.8 keV (2+) starts to be populated significantly only at higher temperatures (6% at kT = 20, 21% at 30 keV). However, the difference between laboratory and stellar cross section grows faster with temperature, because of the larger spin difference. Note, that under these conditions inelastic scattering may accelerate the scattered neutron if the initial state was at higher excitation.

Figure 5 compares the ratio of stellar and laboratory cross sections for those **s**-only isotopes, where this effect exceeds 10% at kT = 30 keV. It illustrates that different calculations are still very discrepant in this respect, and that this effect needs to be studied in more detail. So far, this has been done only for ^{187}Os/39/, which is important for its possible use as a cosmic clock. In this case, the difference between the calculations quoted in figure 5 was even 40% !

In principle, the temperature dependence of stellar cross sections represents a possibility to determine the **s**-process temperature via the well established $\langle\sigma\rangle$N-correlation (see next section).

4. The classical **s**-process: abundances and physical conditions

The most obvious feature of the abundance pattern resulting from the **s**-process is the correlation with cross sections: isotopes with small cross sections will build up to large abundances whereas large cross sections lead to large destruction rates and hence to small abundances. Therefore, the product of stellar cross section and resulting abundance is the characteristic quantity of the **s**-process. Though not completely constant, the product $\langle\sigma\rangle$N is at least a smooth funtion of mass number. This quantity can easily be calculated by means of the classical **s**-process model/1,4/, and is shown in figure 6 for an updated set of input data/27,40,41/.

The classical model is a phenomenological approach, assuming constant neutron density and temperature. In spite of these simplifications, it succeeds to reproduce the empirical $\langle\sigma\rangle$N products for the **s**-only isotopes extremely well. These values are given in figure 6 as symbols with error bars, which include the uncertainties of the respective cross sections and abundances. The fact, that the **s**-process abundances can be reproduced with a precision of ~10% , is a great success for the classical approach, and this success is the more appealing, as this is achieved with only 4 free parameters.

On this basis, the classical model can further be used to investigate more closely the physical conditions during the **s**-process, which are preserved in the **s**-only abundances as well as in the abundance patterns of the **s**-process branchings/42,43/. Being independent of any detailed stellar model, such studies allow to define constraints for the **s**-process site. The significance of these constraints depends on the precision of the model. This means, it depends on (i) the precision of the neutron capture rates, which are the main input data, and on (ii) whether the physical conditions at the stellar site were 'smooth' enough to justify the model assumptions. Given the present uncertainty of ~10% for the $\langle\sigma\rangle$N(A) curve, the second criterion seems still to be satisfied. Only if the relevant capture cross sections will be improved, one might expect to learn more about dynamic aspects of the **s**-process environment from the classical model.

One of these aspects is the influence of temperature. It was discussed in the previous section that the cross sections of some **s**-only

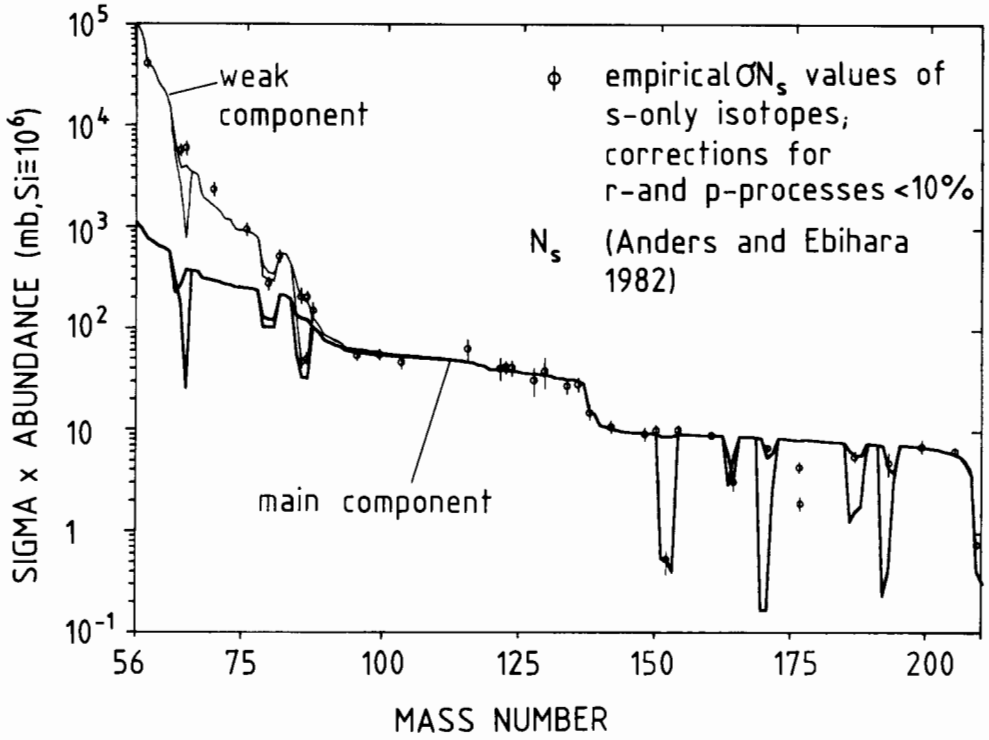

Fig.6 The characteristic product, $\langle\sigma\rangle$N, as a function of mass number. Note, that the empirical products for those isotopes, which originate entirely or predominantly from the **s**-process are reproduced by the classical model (solid lines) within the uncertainties of ~10% . Branchings in the capture chain cause the $\langle\sigma\rangle$N curve to split.

isotopes depend on temperature. This effect may be illustrated again at the example of ^{160}Dy. In figure 6, the empirical <σ>N value of ^{160}Dy agrees exactly with the <σ>N curve. If its cross section were not corrected for the finite population probability of the excited states, the empirical point would fall ~6% below the curve. Because of the 7% uncertainty of the empirical point this difference does not yet allow to use figure 4 as a stellar thermometer; but if the 6% difference were significant, it would indeed yield a temperature of 2.5 10^8 K. This possibility requires more precise laboratory cross sections, but also an improved theoretical conversion to the true stellar values by consideration of the effect of excited states.

While the determination of temperature via the stellar cross sections is limited by the present uncertainties, the before mentioned branchings of the **s**-process path are somewhat more sensitive. The major branchings in the **s**-process path are indicated in figure 6 by the split of the <σ>N curve at the radioactive branching points. As the ratio of neutron capture and beta decay rates of these unstable isotopes defines the strenght of the branching, it is so important to know their capture cross sections as precisely as possible. By systematic branching analyses /43,44,45/, neutron densities and temperatures at the **s**-process site have been determined in this way within factors 2 to 4. Within these uncertainties, the results from individual branchings are still consistent, suggesting that the **s**-process must have been less violent as predicted by stellar models[46].

However, before one can really conclude about the stellar **s**-process, these uncertainties must be further reduced. This definitely requires significant improvement of the input data, in particular of the neutron capture cross sections of the **s**-only isotopes and of the radioactive branching point nuclides. Then, a more precise <σ>N curve and refined branching analyses may yield the neutron density and temperature with an accuracy of 30%, and only then the classical model can yield true constraints for the stellar **s**-process.

References

1. E.M. Burbidge, G.R. Burbidge, W.A. Fowler, F. Hoyle: Rev. Mod. Phys. 29, 547 (1957)
2. P.W. Merrill: Science 115, 484 (1952)
3. W. Hillebrandt: Space Sci. Rev. 21, 639 (1978)
4. G.J. Mathews, R.A. Ward: Rep. Prog. Phys. 48, 1371 (1985)
5. G. Reffo: in Nuclear Theory for Applications Proceedings, Course held at ICTP, Trieste, 17.Jan-10.Feb. 1978)(IAEA, Vienna, 1980), p.205
6. J.W. Truran, F.-K. Thielemann, M. Arnould: Lecture Notes in Physics, Vol. 287: Nuclear Astrophysics, eds. W. Hillebrandt, R. Kuhfuß, E. Müller, J.W. Truran, (Springer, Berlin, 1987) p.91
7. G.J. Mathews, A. Mengoni, F.-K. Thielemann, W.A. Fowler: Ap. J. 270, 740 (1983)
8. E. Lund, K. Aleklett, B. Fogelberg, A. Sangariyavanish: Physica Scripta 34, 614 (1986)
9. R.L. Gill, R.F. Casten, D.D. Warner, A. Piotrowski, H. Mach, J.C. Hill, F.K. Wohn, J.A. Winger, R. Moreh: Phys. Rev. Letters 56, 1874 (1986)
10. K.-L. Kratz, H. Gabelmann, W. Hillebrandt, B. Pfeiffer, K. Schlösser, F.-K. Thielemann and the ISOLDE collaboration, CERN: Z. Phys. A325, 489 (1986)
11. K.-L. Kratz, F.-K. Thielemann, W. Hillebrandt, P. Möller, V. Harms, A. Wöhr, J.W. Truran: Inst. Phys. Conf. Ser. No.88, J. Phys. G, Vol.14 Suppl., S331 (1988)
12. D.D. Clayton: Principles of Stellar Evolution and Nucleosynthesis (McGraw Hill, New York, 1968)
13. M.C. Moxon, E.R. Rae: Nucl. Instr. Meth. 24, 445 (1963)
14. R.L. Macklin, J.H. Gibbons: Phys. Rev. 159, 1007 (1967)
15. F. Corvi, A. Prevignano, H. Liskien, P.B. Smith: Nucl. Instr. Meth. A265, 475 (1988)
16. G.V. Muradyan, Yu.V. Adamchuk, Yu.G. Shchepkin, M.A. Voskanyan: Nucl. Sci. Eng. 90, 60 (1985)
17. K. Wisshak, F. Käppeler: Nucl. Instr. Meth. A227, 91 (1984)
18. K. Wisshak, F. Käppeler, H. Müller: Nucl. Instr. Meth. A251, 101 (1986)
19. K. Wisshak, K. Guber, F. Käppeler, J. Krisch, H. Müller, G. Rupp, F. Voss, contribution AC09, this conference
20. H. Beer, F. Käppeler: Phys. Rev. C21, 534 (1980)
21. W. Ratynski, F. Käppeler: Phys. Rev. C37, 595 (1988)
22. F. Käppeler, A.A. Naqvi, M. Al-Ohali: Phys. Rev. C35, 595 (1987)
23. Yu.V. Petrov, A.I. Shlyakhter: Ap. J. 327, 294 (1988)
24. W.P. Poenitz: J. Nucl. Energy 20, 825 (1966)
25. S. Zhu, S. Jiang, Y. Chen, D. Luo: Chin. J. Nucl. Phys. 6, 23 (1984)
26. F. Käppeler, G. Walter, G.J. Mathews: Ap. J. 291, 319 (1985)
27. Z.Y. Bao, F. Käppeler: At. Data Nucl. Data Tables 36, 411 (1987)
28. R.L. Macklin: Nucl. Sci. Eng. 81, 520 (1982)
29. R.L. Macklin: Astrophys. Space Sci. 115, 71 (1985)
30. R.L. Macklin: Nucl. Sci. Eng. 89, 79 (1985)
31. P.E. Koehler, contr. IJ01, this conference
32. J.A. Holmes, S.E. Woosley, W.A. Fowler W A, B.A. Zimmerman: At. Data Nucl. Data Tables 18, 305 (1978)
33. S.E. Woosley, W.A. Fowler W A, J.A. Holmes, B.A. Zimmerman: At. Data Nucl. Data Tables 22, 371 (1978)
34. M.J. Harris: Astrophys. Space Sci. 77, 357 (1981)
35. G. Reffo, priv. communication (1982)
36. G. Walter, B. Leugers, F. Käppeler, Z.Y. Bao, G. Reffo, F. Fabbri: Nucl. Sci. Eng. 93, 357 (1986)
37. R.R. Winters, F. Käppeler, K. Wisshak, G. Reffo, A. Mengoni: Ap. J. 300, 307 (1986)
38. G. Reffo, F. Fabbri, K. Wisshak, F. Käppeler: Nucl. Sci. Eng. 93, 357 (1982)
39. R.R. Winters, R.F. Carlton, J.A. Harvey, N.W. Hill: Phys. Rev. C34, 840 (1986)
40. E. Anders, M. Ebihara: Geochim. Cosmochim. Acta 46, 2363 (1982)
41. K. Takahashi, K. Yokoi: At. Data Nucl. Data Tables 36, 375 (1987)
42. R.A. Ward, M.J. Newman, D.D. Clayton: Ap. J. Suppl. 31, 33 (1976)
43. F. Käppeler: Inst. Phys. Conf. Ser. No.88, J. Phys. G, Vol.14 Suppl., S297 (1988)
44. H. Beer, G. Walter, R.L. Macklin, P.J. Patchett: Phys. Rev. C30, 464 (1984)
45. F. Käppeler, H. Beer, K. Wisshak: Rep. Prog. Phys. (in preparation)
46. I. Iben Jr.: Ap. J. 208, 165 (1976)